RMIT
UNIVERSITY

Thank you for downloading this document from the RMIT Research Repository.

The RMIT Research Repository is an open access database showcasing the research outputs of RMIT University researchers.

RMIT Research Repository: http://researchbank.rmit.edu.au/

PLEASE DO NOT REMOVE THIS PAGE

Structural Assessment of Microvascular Self-Healing Laminates Using Progressive Damage Finite Element Analysis

Alex T. T. Nguyen [a] and Adrian C. Orifici [a] [*]

[a] RMIT University, School of Aerospace, Mechanical and Manufacturing Engineering,

GPO Box 2476, Melbourne, Victoria 3001, Australia

* corresponding author: adrian.orifici@rmit.edu.au, +61 3 9925 6092, fax +61 3 9925 6108

Abstract

This paper presents a progressive damage analysis methodology to numerically analyse the effect of microvascular open channels on the structural properties of self-healing fibre-polymer laminates. The tensile and compression properties of self-healing carbon-epoxy laminates containing microvascular systems are analysed using finite element models which consider progressive in-plane ply damage and intra-ply damage (matrix and delamination cracking). The models predict with good accuracy (often within 5%) the stiffness and strength of laminates containing circular or elliptical microvascular channels of different sizes and orientations. The model calculates a progressive reduction in structural properties with increasing size of microvascular channels due to increased ply waviness, which was confirmed using experimental property data. The model also predicts the location and progression of damage under increasing tensile or compression loading to final failure. The model has application as a tool for the design of microvascular systems in self-healing composites used for structural applications.

1

1. Introduction

Fibre-reinforced composites have been increasingly used for aircraft structures over the past decades due to their high specific mechanical properties. However, composite structures are susceptible to being easily damaged when subjected to even a low energy impact. This type of damage is hard to inspect and assess, though can cause a significant reduction in compressive strength. Recently, techniques have been developed to detect and autonomically repair internal damage that are based on self-healing composites containing a distributed network of internal microvascular channels for the transport and release of liquid dye or radio-opaque fluid (for damage detection) or healing agent (for repair) [1-4]. These channels, typically with an average diameter in the range 50-500 μm, can be used to sense damage onset, or be filled with liquid resin or catalyst to allow self-healing once a cavity is ruptured. The main idea is to mimic the sensing and healing nature of a living system through a vascular network of internal channels.

Essentially, a microvascular channel can be treated in numerical modelling as an elongated void of constant diameter and infinite length with associated fibre waviness and resin-rich regions in the surrounding laminate material. Experiments on the effect of fibre waviness have shown a 10% to 15% reduction in compressive strength at 8°waviness angle [5-7]. Research on the effect of channels on composite laminates has shown similar results, where Trask et al. [8] and Huang et al. [9] measured a 16% reduction in compressive

strength for a carbon/epoxy material containing a series of 0.6 mm diameter microvascular fibres while Kousourakis et al. [10, 11] found a 15% reduction in strength for a carbon/epoxy laminate containing 0.68 mm diameter microvascular channels. These studies emphasised that microvascular channels alter the microstructure of the laminate by creating localised zones containing resin-rich regions and fibre waviness. These two geometric defects are considered the primary causes of property reduction for composite laminates with microvascular channels, with fibre waviness the dominant aspect.

There has been limited research into assessing the effect of microvascular channels on the mechanical properties of composite using numerical analysis. One important study was reported by Huang et al. [12], who performed finite element (FE) analysis using a representative volume element (RVE) model of the composite material to assess the structural effect of microvascular fibres. Linear static analysis of a plane strain model was used to determine the geometric stress concentration factor around the channel edge. Failure stresses and damage mechanisms were then deduced from the stress concentrations. The use of static analysis required an assumption to ignore any progressive damage effects, which can be important in the failure process controlling strength. Further, the study did not consider the situation where channels are parallel to the applied load.

In this paper, a finite element model incorporating progressive damage analysis is used to assess the effect of microvascular channels on the mechanical properties of self-healing composite materials. Experimental specimens and results from Kousourakis et al. [10] are used to develop the modelling approach. The parameters of the RVE model are presented, including the geometric assumptions, damage models, and effect of mesh

3

density. The model is then used to determine the tension and compression properties for a self-healing [0/90] carbon-epoxy laminate containing circular and elliptical shaped microvascular channels of various sizes and orientations (parallel and transverse to the load direction). The results are compared to experimental results in terms of the stiffness and strength reductions as well as the damage behaviour.

2. Specimen definition

The specimen definition in this work was taken from the experimental investigation of Kousourakis et al. [10], who studied the effect of circular and elliptical channels of various sizes. Removable silicon tubes and non-removable glass tubes were embedded at a pitch of 5 mm to create elliptical and circular channels, as shown in Figure 1 and Figure 2. The result of the different manufacturing techniques meant that the elliptical channels were "bare" while the circular channels were lined with a thin-wall glass tubing. Carbon/epoxy T300/914 unidirectional prepreg material was used in a $[0/90]_{16S}$ laminate, and the channels were embedded at the laminate mid-plane. Under consolidation during curing, the plies were forced to bend around the channels, which led to local fibre waviness and resin-rich zones in the cured laminate, as shown in Figure 1. The ply waviness angle and the area of the resin-rich zone diminished with increasing distance away from the channels. The reader is referred to Kousourakis et al. [4, 10, 11] for further detail on the manufacturing and microstructural characterisation of the materials.

As shown in Figure 2, the specimens were loaded in tension and compression along the longitudinal (Z) direction, which is parallel to the microvascular channels, and along the transverse (X) direction, which is orthogonal to the channels. The average experimental

measurements for the channel geometry were reported in Ref. [10], and are repeated in Table 1 for the specimens considered in this work. In Table 1, $2a$ and $2b$ are hole dimensions (and equal to the outer diameter (OD) for circular channel), θ is the fibre waviness angle, t_{total} is the total laminate thickness and V_f is the average fibre volume content. Channels of different sizes were investigated for each channel type, where the circular channel had an outer diameter of 0.17 mm, 0.32 mm and 0.68 mm, and the elliptical channels were classified in terms of the major axis dimension ($2a$) of 0.58 mm and 0.86 mm.

3. Numerical modelling

Numerical FE models of an RVE were generated with and without channels, as shown in Figure 3, and represented a quarter of a single channel cross-section, based on symmetry. For the models with a channel, the geometry was based on the actual microstructure of the laminate (Figure 1), and in particular on matching the hole dimensions $2a$ and $2b$, and the fibre waviness angle θ. An idealised constant laminate thickness of 4.032 mm was assumed in which each ply had a thickness of 0.126 mm. Ply waviness around the channel was assumed to take the form of a cubic function and was proportional to the channel height. The length of the resin-rich region was dictated by the fibre misalignment angle. The surface plies were assumed to be smooth and without waviness. The ply waviness angle in the through-thickness direction was assumed to reduce linearly from a maximum around the channel to zero at the surface.

Both full-width RVE models and plane strain RVE models were analysed. The plane strain RVE model was used for some transverse loading investigations (such as mesh

sensitivity studies) to assist with computational efficiency. The RVE models used a ply-level meshing scheme with continuum shell elements for the ply layers and solid elements for the glass (circular channels only) and resin-rich regions as shown in Figure 3. The material coordinate system for the ply elements was defined using the element geometry, so that each element had a local coordinate system that was able to capture the waviness in each ply layer. The element coordinate system is given in Figure 4.

Boundary conditions were applied to represent the periodic nature of the RVE model, and were taken from Sun and Vaidya [13]. The boundary conditions are shown in Figure 5, where the periodic boundary conditions were applied by maintaining the displacement of each face plane. Longitudinal loading was applied using $\delta_3 = 0.04$ mm and transverse loading was applied using $\delta_1 = 0.04$ mm. Plane strain transverse loading models were also investigated using one element in the width (Z) direction, and the additional boundary condition of $w = 0$ for all nodes.

The Abaqus progressive damage model for fibre-reinforced composite materials [14] was applied to the ply elements to capture in-plane ply failure modes. In this damage model, damage is categorised into four modes using the Hashin criteria for fibre *(f)* and matrix *(m)* failure in tension *(t,T)* and compression *(c,C)*, using the following equations for the failure index, *F*:

$$F_f^t = \left(\frac{\sigma_{11}}{X_T}\right)^2 + \left(\frac{\tau_{12}}{S_{12}}\right)^2 \qquad \text{for } \sigma_{11} \geq 0; \qquad (1)$$

$$F_f^c = \left(\frac{\sigma_{11}}{X_C}\right)^2 \qquad\qquad \text{for } \sigma_{11} < 0; \qquad\qquad (2)$$

$$F_m^t = \left(\frac{\sigma_{22}}{Y_T}\right)^2 + \left(\frac{\tau_{12}}{S_{12}}\right)^2 \qquad\qquad \text{for } \sigma_{22} \geq 0; \qquad\qquad (3)$$

$$F_f^c = \left(\frac{\sigma_{22}}{2S_{23}}\right)^2 + \left(\left(\frac{Y_C}{2S_{23}}\right)^2 - 1\right)\frac{\sigma_{22}}{Y_C} + \left(\frac{\tau_{12}}{S_{23}}\right)^2 \qquad\qquad \text{for } \sigma_{22} < 0, \qquad\qquad (4)$$

where failure is deemed to initiate when $F = 1$, σ_1, σ_2, τ_{12} are in-plane ply stresses in the fibre coordinate system, X_T, X_C, Y_T, Y_C are in-plane ply strengths in the fibre (X) and transverse (Y) directions, and S_{12} and S_{23} are shear strengths in the in-plane and out-of-plane directions respectively.

Once damage occurs within a ply its stiffness is gradually reduced to zero with increasing strain. This differs from a simple knockdown approach to property reduction, where a gradual reduction is implemented to alleviate mesh sensitivity issues associated with the knockdown approach. The reduction of the stiffness properties is controlled by the area under the stress-displacement curve, as shown in Figure 6. This area is the critical strain energy release rate or "fracture energy" (G_c) for that mode, so that there are four fracture energies required in total. The stiffness reduction depends on the damage mode, where matrix failure triggers reductions in the all terms in the stiffness matrix except C_{11}, whereas fibre failure triggers reduction in all stiffness matrix terms.

It is important to note that this damage model is only available for elements with a plane stress formulation (which includes shells), and only applies to in-plane properties. As such, the damage progression does not affect the out-of-plane properties. For shell elements, this means that the material remains rigid in the out-of-plane direction regardless of the extent of damage.

To investigate interlaminar damage occurring between plies, cohesive elements were included for some models at the interface between ply boundaries. Cohesive elements are interface elements that use a traction-separation material law similar to that represented in Figure 6, except for cohesive elements the properties are controlled in the three orthogonal material directions representing the three crack displacement modes (I – opening, II – sliding shear, III – scissoring shear). As such, the cohesive element material model requires the initial stiffness K (the slope of the traction-separation material law prior to damage), damage initiation traction (stress) σ^0, and the fracture toughness for each of the three modes. To allow for interlaminar damage at any possible location, zero-thickness cohesive element layers were embedded at every ply interface as well as between the resin-rich region and the adjacent ply. Combined application of the damage models for in-plane damage (fibre and matrix failure) and interlaminar damage (delamination) is referred to in this work as the "in-plane and interlaminar damage model".

The material properties applied are given in Table 2, Table 3 and Table 4. The ply elastic and strength properties were taken from Kousourakis et al. [10]. The ply fracture energies for the material used were not available, so values from taken from Kärger et al. [15] for a similar material system. For the cohesive element properties, the fracture

toughness values and damage initiation stresses were taken from Kousourakis et al. [11]. The stiffness in all directions was taken from recommendations from Ref. [16] as a compromise between high stiffness and ease of computational convergence. The calculated cohesive zone length is 3.05 mm and the maximum element length in any model was around 0.126 mm. In this way, all models used many more than the recommended minimum of three elements in the crack growth direction, and separately avoided the infeasible situation where the total fracture energy is less than the elastic energy up to failure initiation.

Using the RVE modelling approach, investigations were conducted using the in-plane damage model only, and combining the interlaminar and in-plane damage models. All models were run on an i7 processor, with a typical analysis time of 0.5 hours for all analyses.

4. In-plane damage model analysis

An investigation was conducted into the effect of mesh density using the in-plane damage model. This was followed by an analysis of all configurations, in comparison with the experimental results.

4.1. Mesh sensitivity study

The mesh sensitivity study for in-plane damage considered only the 0.68 mm circular channel specimen with transverse loading and plane strain conditions. The model shown in Figure 3a was meshed with one element in the ply thickness direction, or an element length of 0.126 mm in the thickness direction, with approximately square elements. Additional

9

models were generated based on doubling the number of elements (n) in the thickness direction in each ply and maintaining approximately square elements, so that models with 2, 4, 8 and 16 elements per ply thickness were also investigated. This reduced the element length in the thickness direction from 126 μm to 7.8 μm for the finest mesh model.

The results of the mesh density investigation are shown in Figure 7 and Figure 8, where Figure 7 shows the stress-strain results for all models and Figure 8 compares the fibre fracture damage index for two mesh densities, where the damage index for this and subsequent similar figures is between 0 (no damage) and 1 (fully damaged). The stress-strain results show that the behaviour of each model involved an approximately linear region, a region of approximately constant stress, then a rapid loss of load. From the results, the maximum load reached by all models was almost identical and corresponded to the end of the linear region. Further, reducing the element length only brought the rapid load loss closer to the point of maximum load. A comparison of a coarse and fine mesh in Figure 8 shows that the damage pattern was identical in both cases, and involved fibre fracture initiating at the hole and progressing rapidly in the through-thickness direction towards the surface.

From considering the experimental behaviour, and from the brittle nature of the material, it is expected that the model should show catastrophic failure upon reaching maximum load, rather than the large plateau of high loads seen for coarse meshes. This indicates that smaller elements more accurately represented the experimental behaviour. This is likely due to the fact that the damage model does not reduce the stiffness of each element in the thickness direction, which remains rigid due to the assumption of plane

stress. As such, a high density of elements in the thickness direction is required to capture the damage along the through-thickness damage path that causes the rapid loss of load. With a reduced element length in the thickness direction, the model is more able to capture the through-thickness damage path and load transfer using the damage to the in-plane properties. Despite this, the results clearly showed that the ultimate load for the RVE could be taken from even the coarsest mesh model. Comparatively, the overall computational time of the 16 elements per ply model was 240 hours in comparison with 0.5 hours for the one element per ply model.

A separate investigation was conducted to compare a plane strain model using one element in the width (Z) direction to a model of the full width RVE. From this, it was found that the plane strain model produced almost identical results to a full width model.

4.2. Results and discussion

A detailed investigation using the in-plane damage model was conducted considering all channel sizes and types (including the no channel configuration) in comparison with experimental results. A full RVE model (quarter symmetry) was used with one element in the ply thickness direction. The results of the investigation are summarised in Table 5 for the no channel model, Table 6 for differences in stiffness and Table 7 for the differences in strength, where stiffness is the slope of the linear portion of the stress-strain results. A sample of the stress-strain results is shown for the 0.68 mm circular channel in transverse loading in Figure 9, where the initiation of different damage modes is also indicated. A sample of the fibre fracture damage patterns following ultimate load is shown in Figure 10.

11

For the no channel model, the results in Table 5 show that the model gave very close predictions of the experimental results for both stiffness and strength. However, the experimental strength results were used as input to the numerical model material properties, so these results merely confirm the suitability of the RVE approach. In the rest of this work, only the results for models with channels are discussed, and the no channel results are used in a later section as baseline results to assess the structural effect of introducing the channels.

In terms of stiffness results in Table 6, the numerical predictions for the models with channels were all within 10% of the experimental results. For the configurations in tension the numerical models generally under-predicted the experimental stiffness within 5%. On the other hand, for the compression configurations the numerical models generally over-predicted the experimental stiffness. For transverse compression, the numerical predictions were within 5%, whereas for longitudinal compression the predictions were within 10%. The results showed that in general the numerical models gave accurate predictions of the stiffness, and were able to represent the structural effect of fibre waviness on the laminate stiffness.

For the strength results in Table 7, all predictions using the RVE model correlate well with experimental data from Kousourakis et al. [10]. Predictions for all load cases and all channel sizes except the largest elliptical channel are within 10% of the experimental results, and the majority are within 5%. This is within the scatter seen in experimental testing, and demonstrates the capabilities of the in-plane progressive damage model to capture the stress concentration effects produced by the channel geometry.

12

In terms of specimen behaviour, the models loaded in the transverse direction showed matrix damage and fibre damage initiating well before the ultimate load was reached, as illustrated in Figure 9 and Figure 10a for the transverse tension case. The fibre failure initiated at the hole edge at the maximum stress, which for the circular channels was at a location approximately 30° relative to the top of the hole, as seen in Figure 10a. The fibre failure then progressed in the through-thickness direction, moving first towards then away from the specimen symmetry axis. For the elliptical channels in transverse compression, failure progressed only away from the symmetry axis as shown in Figure 10b. This general failure pattern under transverse loading was seen for all mesh densities, hole sizes and hole shapes. This demonstrates that the failure under transverse loading has a progressive nature that is dominated by the stress concentration caused by the fibre waviness in the loading direction.

In longitudinal loading, matrix damage was similarly initiated well before the ultimate load, but the first occurrence of fibre failure was very close to the ultimate load. This was due to the fact that there was no fibre waviness in the loading direction, so all plies in the same orientation had the same stress. For longitudinal transverse loading, the failure path was similar to the transverse case, with fibre failure starting at the hole and progressing in the through-thickness direction, though with a more diagonal failure path as shown in Figure 10c. For transverse compression loading, all load-bearing plies failed at the same load as shown in Figure 10d.

More broadly, the numerical models showed slightly poorer predictions for the elliptical channels in comparison with the circular channels. This was likely due to the

increased variability seen in the manufacture of these specimens, and the difficulty in capturing this variation and complexity in the numerical model. The elliptical channels were manufactured using a removable circular silicon tube that under curing pressure was deformed into an elliptical shape. These silicon tubes were removed after cure leaving a higher level of porosity, bulging in the laminate and a non-uniform distribution of fibre waviness through the cross-section. The elliptical shape is also an approximation of the real channel shape, and slight variations in this shape were seen [4, 10, 11]. On the other hand, as the circular channels were formed using rigid glass tubes, the distribution of fibre waviness was uniform for all channel sizes and the models more closely represented the experimental geometry, leading to more accurate predictions.

5. In-plane and interlaminar damage model analysis

Using the combination of the in-plane and interlaminar damage models, an investigation was first conducted into the effect of mesh density. This was followed by an analysis of the transverse loading configurations, in comparison with the in-plane damage model and the experimental results.

5.1. Mesh sensitivity study

The mesh sensitivity investigation for the in-plane and interlaminar damage model was conducted using the 0.68 mm circular channel laminate with transverse tension loading. Plane strain models were analysed with one, two and four elements per ply thickness, with typical element lengths of 0.126 mm, 0.05 mm and 0.0125 mm respectively.

The results of the mesh sensitivity study for in-plane and delamination damage model are shown in Figure 11, where the stress-strain results are presented. The results show a similar character to the results with the in-plane damage model, except instead of a plateau following ultimate load a gradual load reduction is seen. This gradual reduction is attributed to the progression of damage in the cohesive element layers, whereas the catastrophic loss is caused by the in-plane damage model causing a through-thickness damage path. As with the in-plane damage model, the ultimate load of all three meshes is almost identical and reducing the element lengths only made the catastrophic load loss occur closer to the ultimate load. Based on this, and similar reasoning as discussed in the previous section, the model with one element per ply thickness ($n = 1$) was used for all the subsequent analysis with cohesive elements.

5.2. Results and discussion

An investigation into the transverse loading cases was conducted for all channel sizes and types. Only the transverse loading configurations were considered, as these had a higher propensity for delamination due to straightening or buckling of the load-bearing fibres and less favourable comparison with experiment. Plane strain models were applied, with cohesive element layers embedded at every ply interface. The numerical strength values for all configurations analysed are presented in Table 8. Figure 12 shows a sample stress-strain result with the initiation of damage modes indicated, and Figure 13 shows a sample of fibre fracture damage patterns following ultimate load.

Overall, from the strength results in Table 8, application of the in-plane and interlaminar damage model gave close predictions of the experimental ultimate load, though the predictions were similar to those using the in-plane damage model (Table 7).

In terms of damage mode, the in-plane and interlaminar damage model predicted delamination to occur as the first damage mode. This led to the other damage modes occurring earlier than previously predicted with only the in-plane damage model. An illustration of this is seen in Figure 12, where the damage mode initiation is highlighted for the 0.68 mm circular channel in transverse tension, which can be compared to results previously shown in Figure 9. Despite the early onset of delamination, extensive delamination throughout the laminate was typically not seen, resulting in only small reductions in ultimate load across all configurations. This agrees with experimental observations, where very little indication of delamination was seen [10].

Importantly, the application of the in-plane and interlaminar damage model resulted in a change of failure path. As shown in the fibre fracture patterns in Figure 13, fibre fracture initiated at the top of the hole and progressed in the through-thickness direction of the laminate. This damage pattern agrees more closely with the experimental results, examples of which are shown in Figure 14, where a fracture path initiating at the side of the hole and progressing directly to the laminate edge was seen [10]. This indicates that incorporating delamination is necessary in order to capture the specimen behaviour, as is a progressive damage approach allowing for the interaction between in-plane and interlaminar damage modes.

6. Structural effect of internal channels

The numerical predictions from using the in-plane damage model are normalised with respect to the corresponding strength or stiffness from the no channel model in order to assess the structural effect of introducing channels into the composite laminate. These results are presented in Figure 15 for stiffness and Figure 16 for strength, ordered in terms of increasing fibre waviness angle.

The results show a roughly linear relation between knockdown factor and waviness angle that is independent of the channel geometry (i.e. circular or elliptical). This demonstrates the critical contribution the waviness angle makes to the laminate performance, regardless of channel type. In terms of channel size, increasing the channel size leads to a greater reduction in mechanical properties. For equivalent area channels such as the 0.68 mm circular channel and the 0.86 mm elliptical channel, the circular channels have a higher waviness angle as the elliptical channel is flattened on the top and bottom

17

surface. Thus, greater reductions in strength occur with the circular channels compared to the elliptical channels for similar cross sectional areas.

The reduction in mechanical properties is also dependent on the loading direction. When the loading is parallel to the channel, the load-carrying fibres are straight, so that small reductions of around 5% are calculated for strength and stiffness. These reductions are mainly contributed by the reduced load-bearing area. On the other hand, under transverse loading the load-carrying plies have a non-straight load path, leading to larger property reductions, for example a 15% reduction in strength and 9% reduction in stiffness for the largest circular channel.

7. Conclusion

A numerical analysis approach for assessing the structural effect of embedding channels within a composite laminate was developed and demonstrated. An RVE model was analysed in Abaqus using damage models for in-plane and interlaminar damage. As the ply damage model considered in-plane damage, whilst the crack path through the model was in the through-thickness direction, a high mesh density was required to capture realistic behaviour post-ultimate load. Further, incorporation of delamination using cohesive elements was found to provide accurate predictions of the damage patterns observed experimentally. Despite this, coarse mesh models with only in-plane damage captured were found to be suitable for ultimate load predictions. The numerical analysis approach gave close comparison with experimental results for circular and elliptical embedded channels of different sizes up to nearly 1 mm.

Using the numerical models, the structural effect of embedding channels was assessed within the range of channel types and sizes considered. Under longitudinal loading (parallel to the channel), there is a modest reduction in strength and stiffness of the laminate with internal channels as the load-carrying plies remain undistorted. However, under transverse loading, the load-carrying plies no longer have a straight load path and thus the strength and stiffness of the laminate is reduced significantly. The reductions in stiffness and strength of the various channel configurations were quantified as property knockdown factors, and the fibre waviness angle was highlighted as a key geometry parameter for structural performance.

The result of this work have application for the design and analysis of laminates with internal channel networks, in terms of demonstrating successfully numerical analysis strategies, and the effect of various channel sizes and shapes on structural behaviour.

Acknowledgments

References

[1] White SR, Sottos NR, Moore JS, Esser-Kahn AP, Thakre P, Dong H, Patrick JF. Multi-functional microvascular composite materials, 18th International Conference on Composite Materials, 21-26 August, Jeju Island, South Korea, 2011.

[2] Aragón AM, Smith KJ, Geubelle PH, White SR. Multi-physics design of microvascular materials for active cooling applications. Journal of Computational Physics. 2011;230:5178-98.

[3] Knipprath C, McCombe GP, Trask RS, Bond IP. Predicting self-healing strength recovery using a multi-objective geneticalgorithm. Composites Science and Technology. 2012;72:752-9.

[4] Kousourakis A, Mouritz AP. The effect of self-healing hollow fibres on the mechanical properties of polymer composites. Smart Materials & Structures. 2011;19:1-9.

[5] Garnich MR. Localized fiber waviness and implications for failure in unidirectional composites. Journal of Composite Materials. 2005;39:1225-45.

[6] Mandell JF, Samborsky DD, Wang L. Effects of fibre waviness on composites for wind turbine blades, 48th International SAMPE Symposium, 11-15 May, Long Beach, CA, USA, 2003.

[7] Wang L. Effects of in-plane fibre waviness on the static and fatigue strength of fibreglass. Master of Science thesis, Montana State University; 2001.

[8] Trask RS, Williams HR, Bond IP. Self-healing polymer composites: mimicking nature to enhance performance. Bioinspiration & Biomimetics. 2007;2:1-9.

[9] Huang H, Talreja R. Effects of void geometry on elastic properties of unidirectional fiber reinforced composites. Composites Science and Technology. 2005;65:1964-81.

[10] Kousourakis A, Bannister MK, Mouritz AP. Tensile and compressive properties of polymer laminates containing internal sensor cavities. Composites Part A: Applied Science and Manufacturing. 2008;39:1394-403.

[11] Kousourakis A, Mouritz AP, Bannister MK. Interlaminar properties of polymer laminates containing internal sensor cavities. Composite Structures. 2006;75:610-8.

[12] Huang C-Y, Trask RS, Bond IP. Characterization and analysis of carbon fibre-reinforced polymer composite laminates with embedded circular vasculature. Journal of The Royal Society Interface. 2010;7:1229-41.

[13] Sun CT, Vaidya RS. Prediction of composite properties from a representative volume element. Composites Science and Technology. 1996;56:171-9.

[14] Abaqus® 6.10 Documentation. Providence, RI, USA: Dassault Systèmes Simulia Corporation; 2010.

[15] Kärger L, Baaran J, Gunnion AG, Thomson RS. Evaluation of impact assessment methodologies. Part II: Experimental validation. Composites Part B: Engineering. 2009;40:71-6.

[16] Turon A, Dávila CG, Camanho PP, Costa J. An engineering solution for mesh size effects in the simulation of delamination using cohesive zone models. Engineering Fracture Mechanics. 2007;74:1665-82.

List of figures

Table 1: Specimen experimental average parameters

Channel	$2a$	$2b$	θ	t_{total}	V_f (%)
No channel				4.10	60.0
Circular	0.17	0.17	1.3	4.13	59.9
Circular	0.32	0.32	3.5	4.13	59.8
Circular	0.68	0.68	8.0	4.18	59.1
Elliptical	0.58	0.22	2.4	4.20	59.7
Elliptical	0.86	0.34	4.8	4.27	59.4

Table 2: Material properties of T300/914 unidirectional pregreg

Property	Value	Property	Value
E_{11}	155 GPa	X_T	1610 MPa
E_{22}	10.78 GPa	X_C	1150 MPa
G_{12}	5.65 GPa	Y_T	34 MPa
G_{13}	5.65 GPa	Y_C	200 MPa
G_{23}	3.55 GPa	S_{12}	80 MPa
ν_{12}	0.3	S_{23}	80 MPa
ν_{13}	0.3	ρ	1.59 g/cm^3
ν_{23}	0.381		

Table 3: In-plane fracture toughness values (kJ/mm^2) for the UD ply

Property	Value
G_{ft}	91
G_{fc}	79
G_{mt}	0.15
G_{mc}	0.45

Table 4: Cohesive element properties

Property	Value
K_I	10^6 N/mm
K_{II}	10^6 N/mm
K_{III}	10^6 N/mm
$\sigma_{max, I}$	50 MPa
$\sigma_{max, II}$	88 MPa
$\sigma_{max, III}$	88 MPa
G_I	0.55 kJ/mm^2
G_{II}	0.65 kJ/mm^2
G_{III}	0.65 kJ/mm^2

Table 5: In-plane damage model, strength and stiffness results (MPa) of the no channel model, experiment (exp), FE and difference (%)

	Exp	FE	%
X_T	815	810	0.6
X_C	610	610	0.0
E_{1T}	80	80	0.0
E_{1C}	76	80	-5.3

Table 6: In-plane damage model, stiffness results (MPa) of circular and elliptical channels, experiment (exp), FE and difference (%)

Circular	OD = 0.17 mm			OD = 0.32 mm			OD = 0.68 mm		
	Exp	FE	%	Exp	FE	%	Exp	FE	%
E_{1T}	79	76.5	-3.2	76	76.3	0.4	74	74	0.0
E_{1C}	75	81.3	8.4	74	80.8	9.2	75	78.5	4.7
E_{2T}	79.1	76.4	-3.4	77.4	75.5	-2.5	71.4	69.6	-2.5
E_{2C}	79.3	81	2.1	77.6	79.6	2.6	70	73	4.3
Elliptical	2a = 0.58 mm			2a = 0.86 mm					
	Exp	FE	%	Exp	FE	%			
E_{1T}	79.5	77.1	-3.0	76	76.8	1.1			
E_{1C}	75	81.6	8.8	74	81.4	10.0			
E_{2T}	79.2	76.5	-3.4	76.4	75	-1.8			
E_{2C}	79.3	80.6	1.6	76.4	78.7	3.0			

Table 7: In-plane damage model, strength results (MPa) of circular and elliptical channels, experiment (exp), FE and difference (%)

Circular	OD = 0.17 mm			OD = 0.32 mm			OD = 0.68 mm		
	Exp	FE	%	Exp	FE	%	Exp	FE	%
X_T	815	805	-1.2	800	785	-1.9	830	760	-8.4
X_C	580	605	4.3	590	594	0.7	580	573	-1.2
Y_T	800	790	-1.3	750	755	0.7	680	690	1.5
Y_C	590	585	-0.8	550	575	4.5	510	520	2.0
Elliptical	2a = 0.58 mm			2a = 0.86 mm					
	Exp	FE	%	Exp	FE	%			
X_T	790	795	0.6	790	791	0.1			
X_C	590	601	1.9	590	582	-1.4			
Y_T	810	752	-7.2	775	740	-4.5			
Y_C	610	580	-4.9	610	568	-6.9			

Table 8: In-plane and interlaminar damage model, strength results (MPa) of circular and elliptical channels, experiment (exp), FE and difference (%)

Circular	OD = 0.17 mm			OD = 0.32 mm			OD = 0.68 mm		
	Exp	FE	%	Exp	FE	%	Exp	FE	%
Y_T	800	770	-3.8	750	750	0.0	680	678	-0.3
Y_C	590	573	-2.9	550	560	1.8	510	500	-2.0
Elliptical	2a = 0.58 mm			2a = 0.86 mm					
	Exp	FE	%	Exp	FE	%			
Y_T	810	758	-6.4	775	727	-6.2			
Y_C	610	570	-6.6	610	568	-6.9			
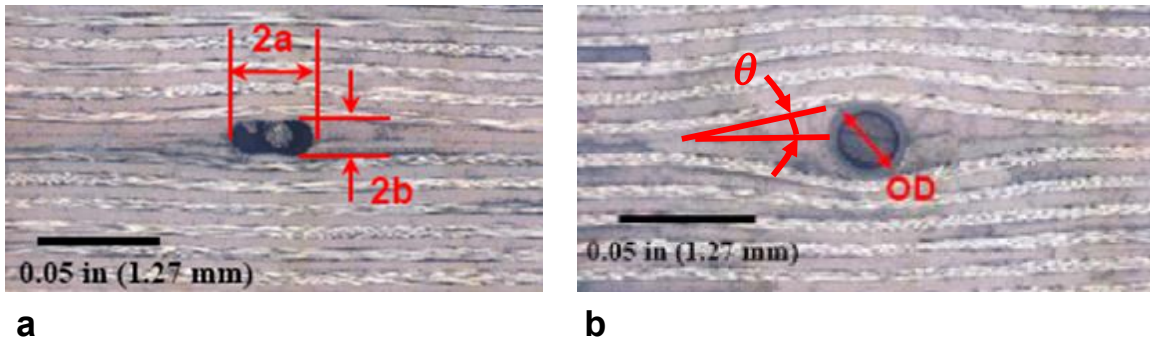
Figure 1: SEM image of internal channels, with geometry parameters labelled. a) Elliptical channel b) Circular channel, showing outer diameter (OD) and fibre misalignment angle [10]
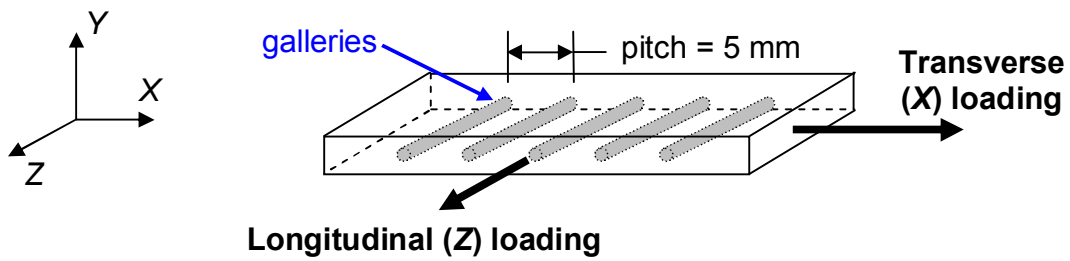
Figure 2: Test specimen, coordinate systems and loading definition (adapted from [10])
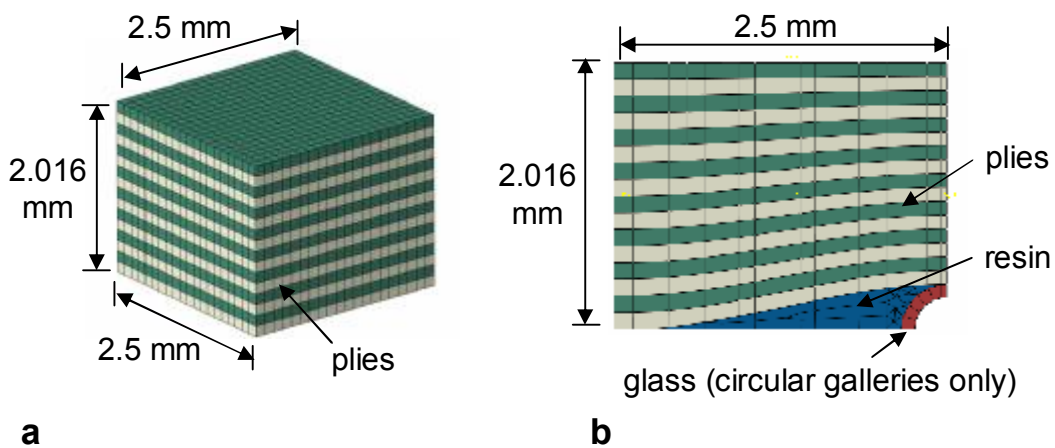
Figure 3: RVE definition. a) No channel model. b) Model with channel (circular channel shown).
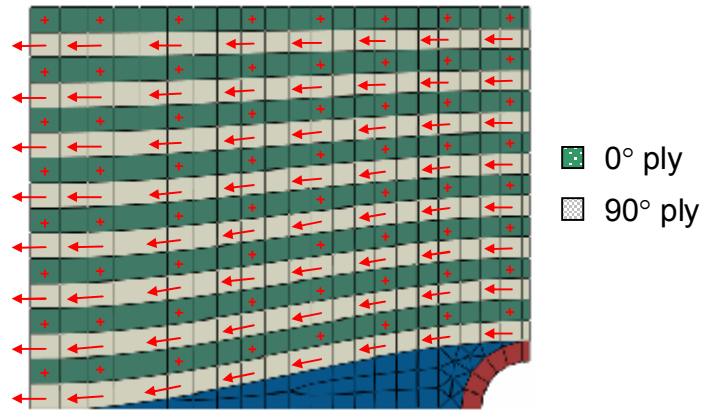
Figure 4: Ply material orientation using element geometry (selected elements shown for clarity)
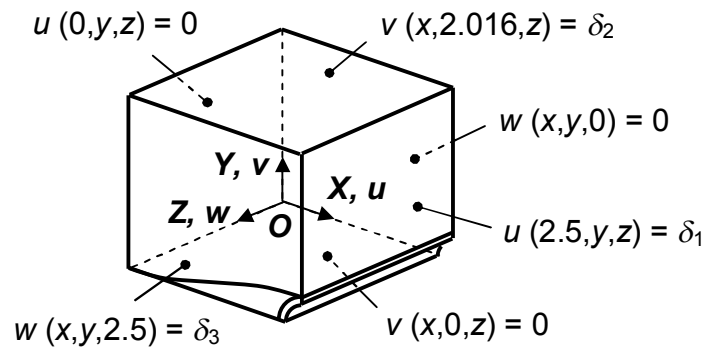
Figure 5: RVE boundary conditions.
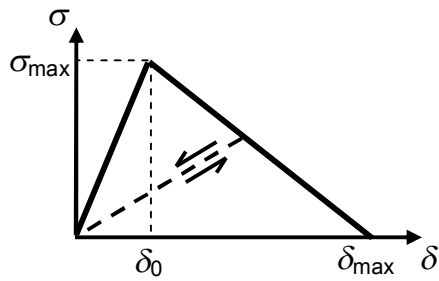
Figure 6: Traction-separation law
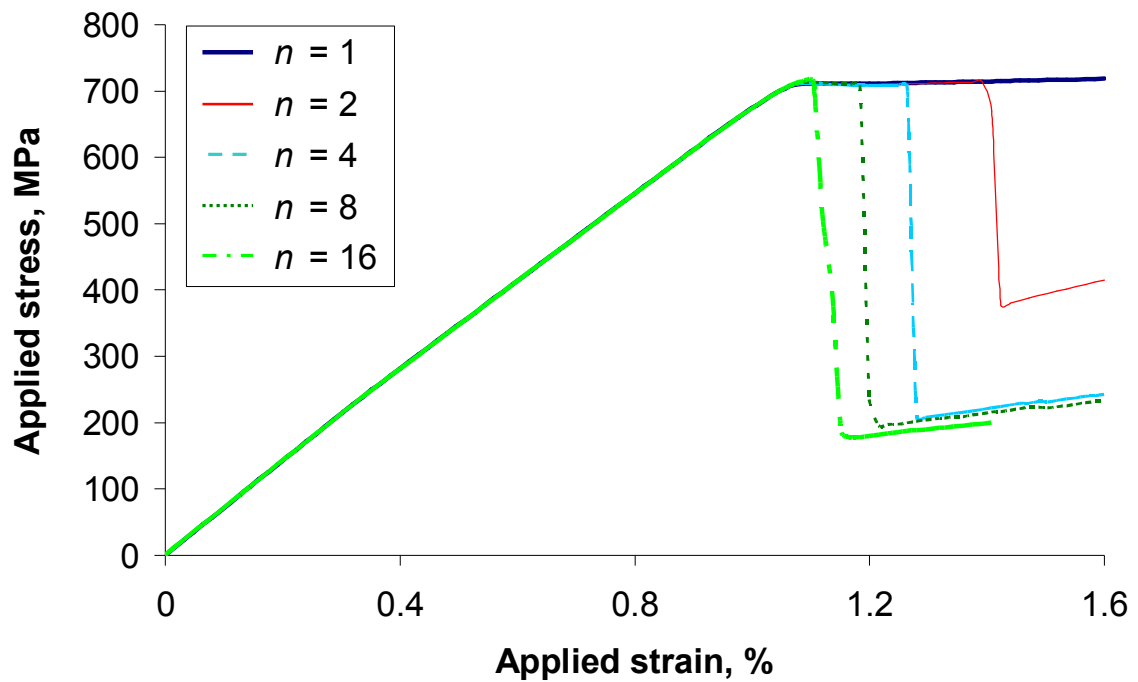
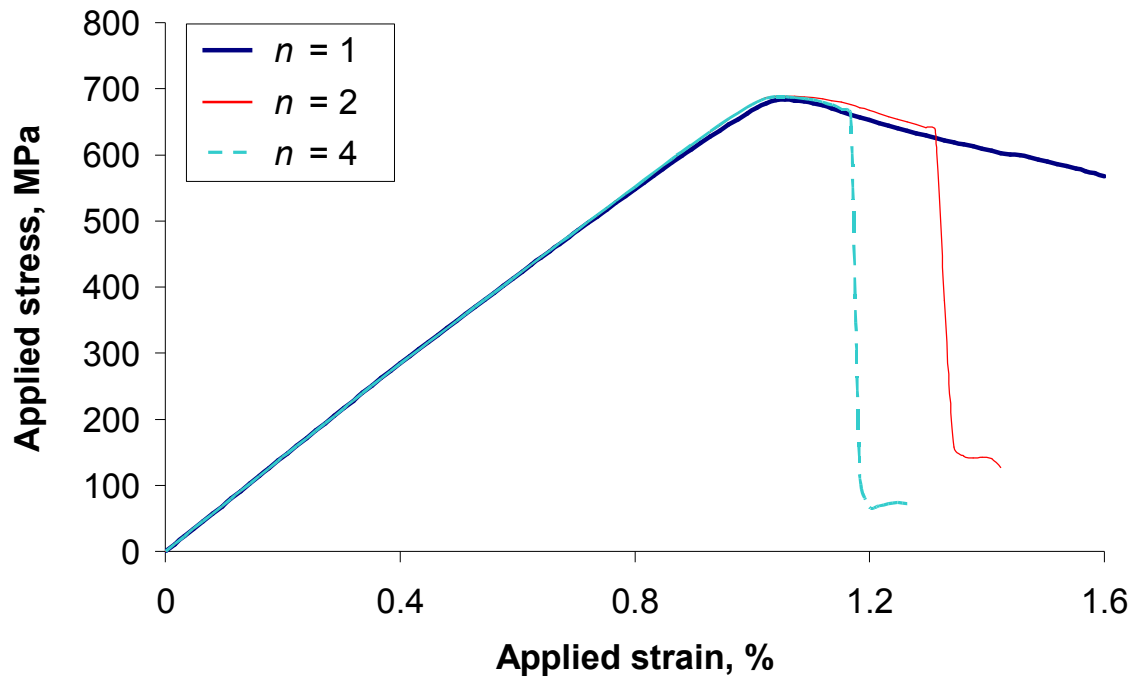Figure 7: In-plane damage model, stress-strain results, 0.68 mm circular channel, transverse tension, varying mesh density (number of elements, n, in the thickness direction per ply).
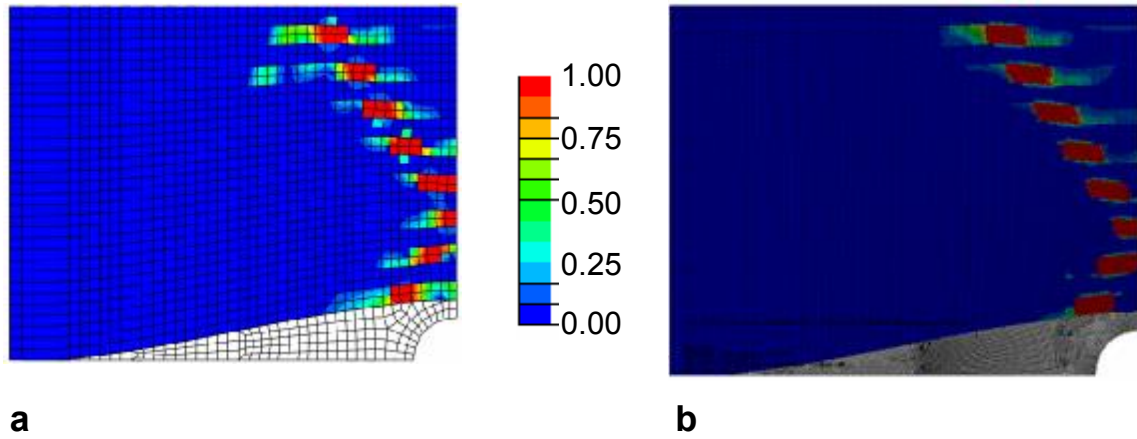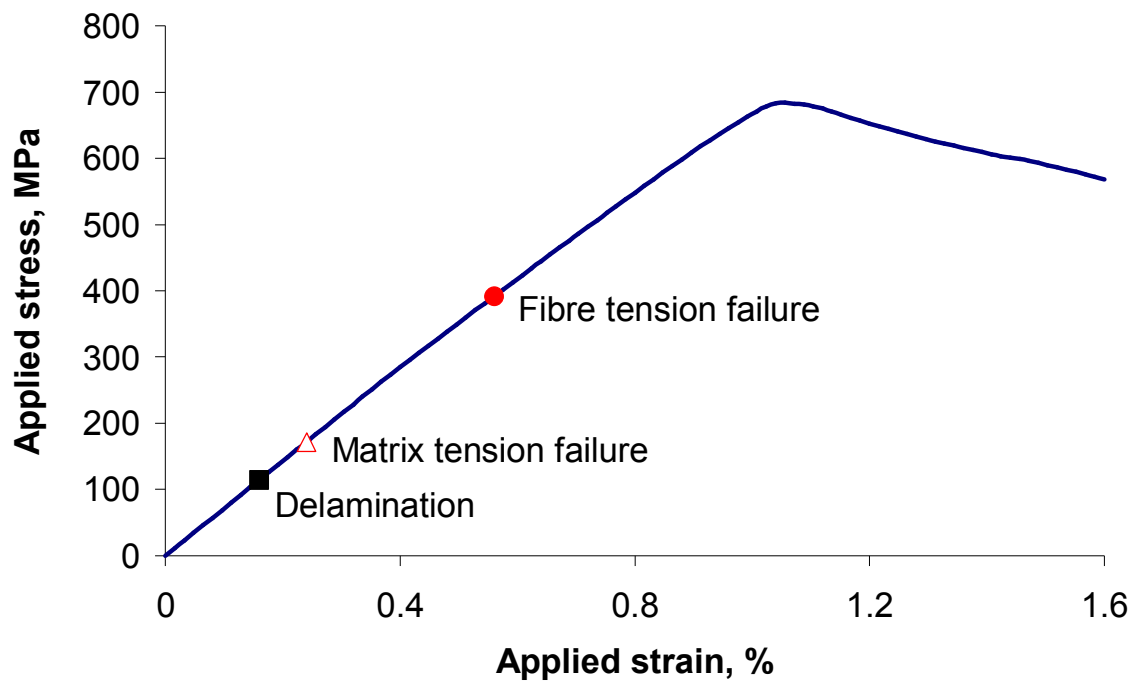
Figure 8: In-plane damage model, fibre fracture damage index, 0.68 mm circular channel, transverse tension. a) $n = 2$. b) $n = 16$.
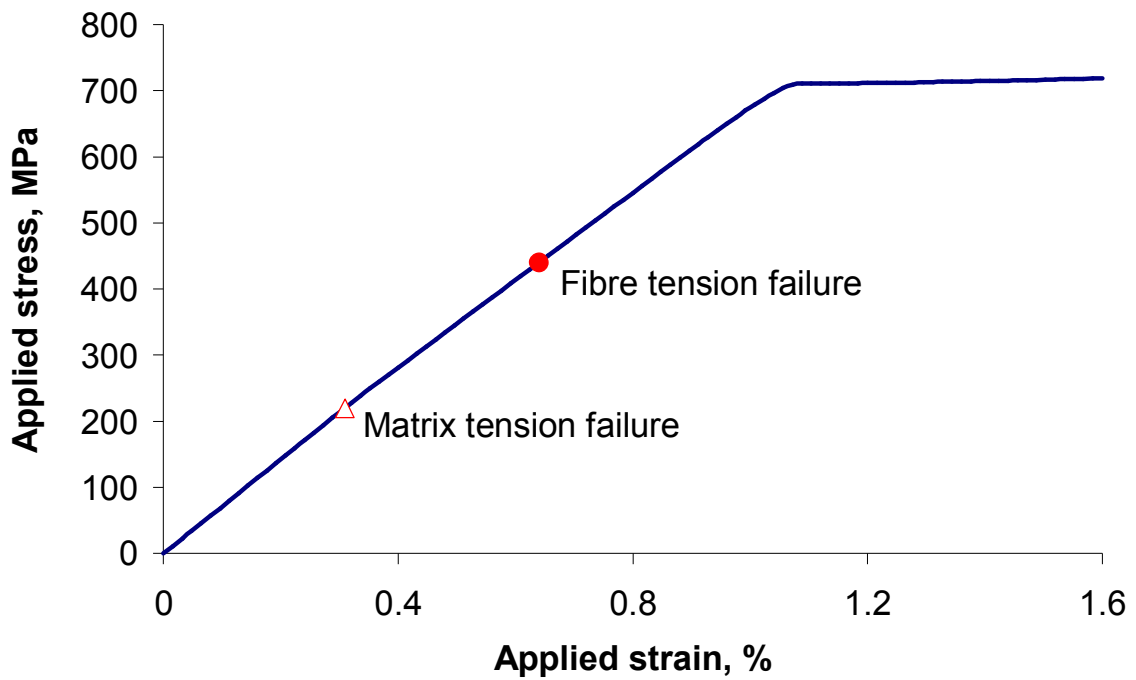
Figure 9: In-plane damage model, stress-strain results with damage mode initiation indicated, 0.68 mm circular channel, transverse tension.
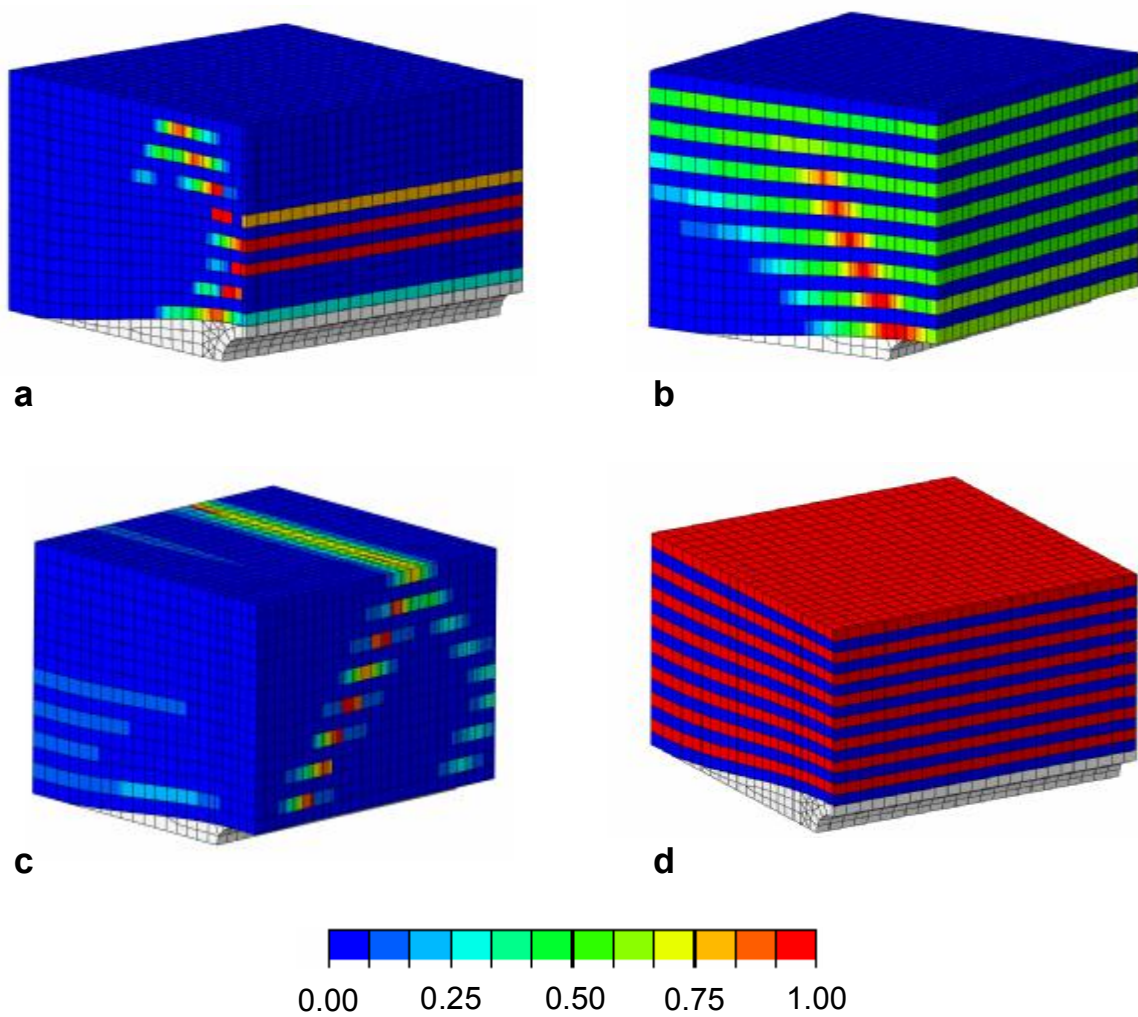
Figure 10: In-plane damage model, fibre fracture damage index following ultimate load. a) 0.68 mm circular channel, transverse tension. b) 0.86 mm elliptical channel, transverse compression. c) 0.86 mm elliptical channel, longitudinal tension. d) 0.68 mm circular channel, longitudinal compression.

Figure 11: In-plane and interlaminar damage model, stress-strain results, 0.68 mm circular channel, transverse tension, varying mesh density (number of elements, n, in the thickness direction per ply).

Figure 12: In-plane and interlaminar damage model, stress-strain results with damage mode initiation indicated, 0.68 mm circular channel, transverse tension.
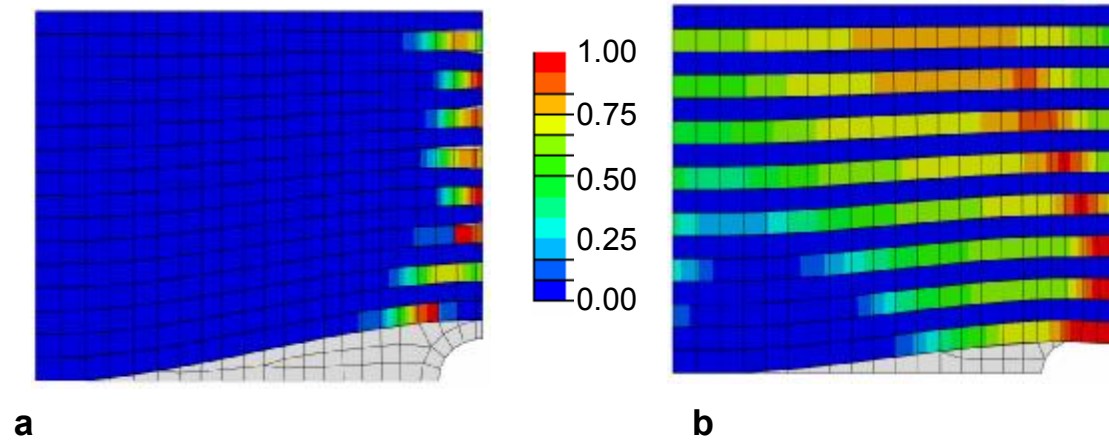
Figure 13: In-plane and interlaminar damage model, fibre fracture damage index following ultimate load. a) 0.68 mm circular channel, transverse tension. b) 0.86 mm elliptical channel, transverse compression.
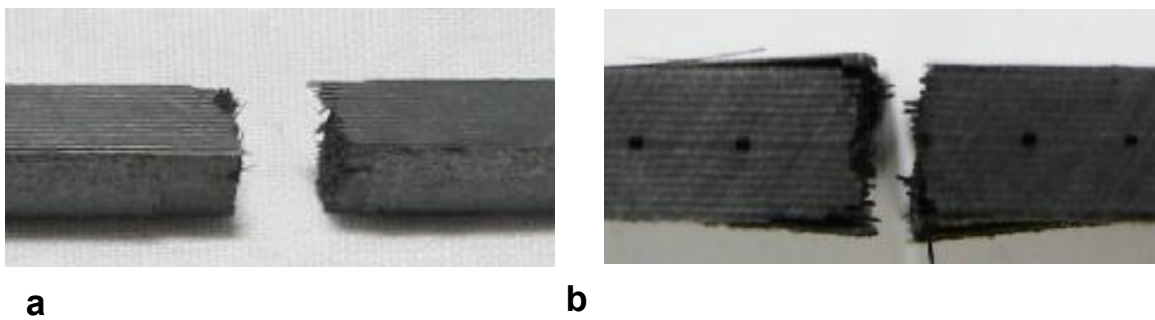

Figure 14: Experimental damage patterns [10]. a) Longitudinal tension, 0.58 mm elliptical channel. b) Transverse tension, 0.58 mm elliptical channel.
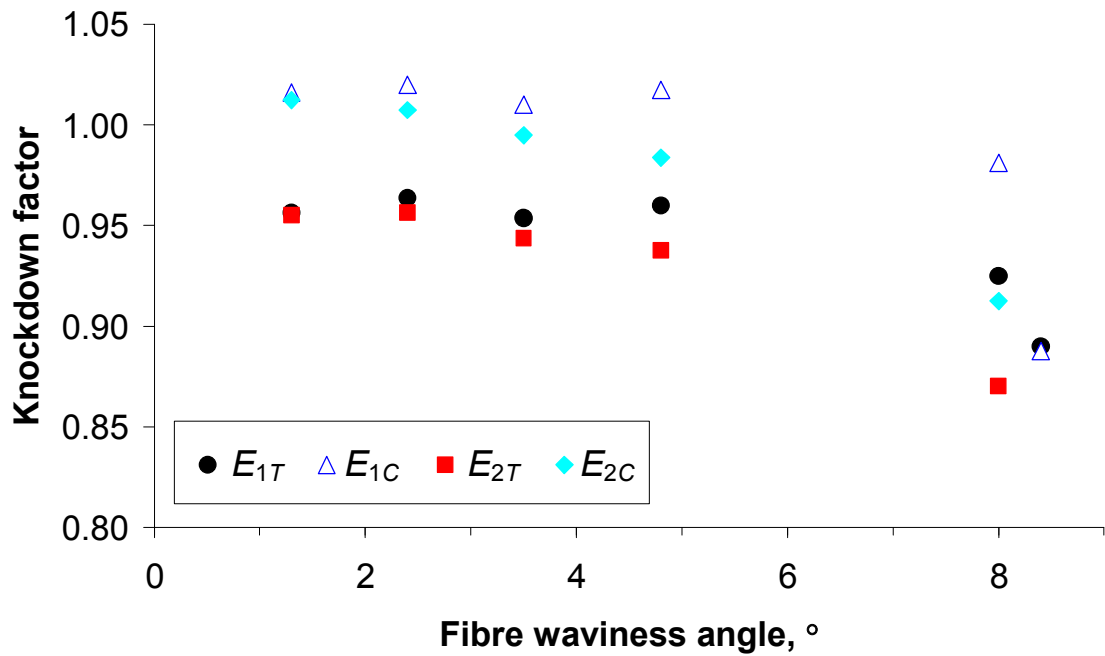
Figure 15: Stiffness knockdown factors (relative to no channel case), in-plane damage model.
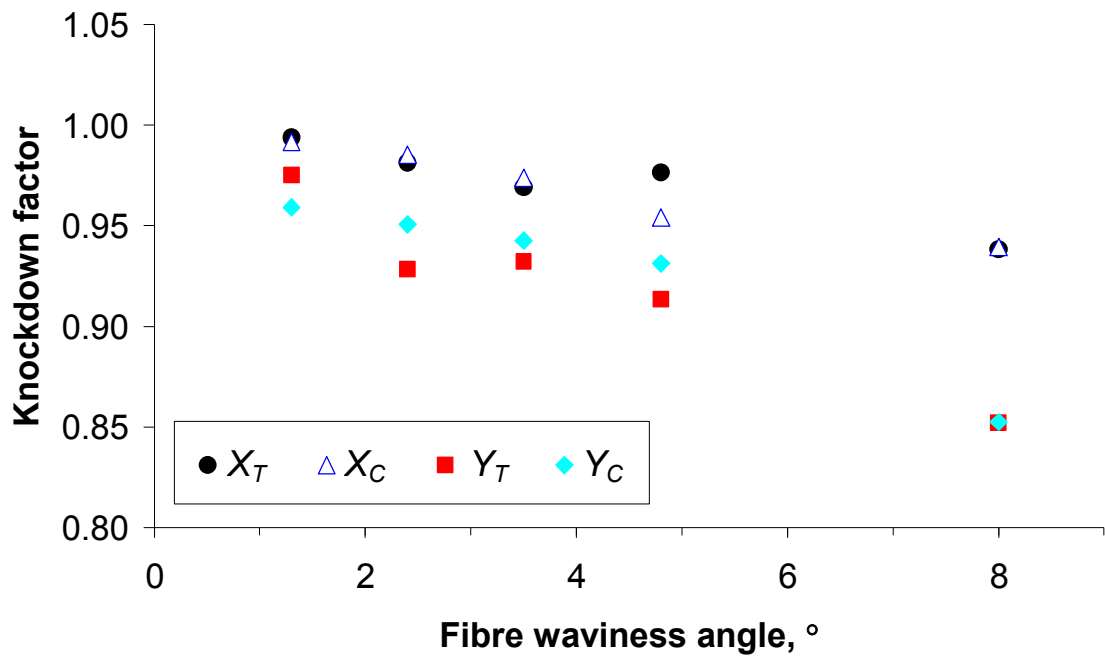

Figure 16: Strength knockdown factors (relative to no channel case), in-plane damage model.